Developmental Cell
Resource

Conditional Knockouts Generated by Engineered CRISPR-Cas9 Endonuclease Reveal the Roles of Coronin in *C. elegans* Neural Development

Zhongfu Shen,[1,3] Xianliang Zhang,[1,3] Yongping Chai,[1,3] Zhiwen Zhu,[1] Peishan Yi,[1] Guoxin Feng,[1] Wei Li,[2] and Guangshuo Ou[1,*]
[1]Tsinghua-Peking Center for Life Sciences, School of Life Sciences, Tsinghua University, Beijing 100084, China
[2]School of Medicine, Tsinghua University, Beijing 100084, China
[3]Co-first author
*Correspondence: guangshuo.ou@gmail.com
http://dx.doi.org/10.1016/j.devcel.2014.07.017

SUMMARY

Conditional gene knockout animals are valuable tools for studying the mechanisms underlying cell and developmental biology. We developed a conditional knockout strategy by spatiotemporally manipulating the expression of an RNA-guided DNA endonuclease, CRISPR-Cas9, in *Caenorhabditis elegans* somatic cell lineages. We showed that this somatic CRISPR-Cas9 technology provides a quick and efficient approach to generate conditional knockouts in various cell types at different developmental stages. Furthermore, we demonstrated that this method outperforms our recently developed somatic TALEN technique and enables the one-step generation of multiple conditional knockouts. By combining these techniques with live-cell imaging, we showed that an essential embryonic gene, Coronin, which is associated with human neurobehavioral dysfunction, regulates actin organization and cell morphology during *C. elegans* postembryonic neuroblast migration and neuritogenesis. We propose that the somatic CRISPR-Cas9 platform is uniquely suited for conditional gene editing-based biomedical research.

INTRODUCTION

The capacity to modify a genomic target in a conditional manner is urgently needed to understand the mechanisms of metazoan development and human disease (Capecchi, 2005). Conditional knockout techniques enable the determination of the function of embryonically lethal genes in postembryonic development and the differentiation of the complex roles of one gene in multiple events, such as the regulation of the cell cycle and/or neural development (Capecchi, 2005). Although DNA recombinase-based Cre-*LoxP* and Flp-*FRT* systems have been widely used to generate conditional knockouts across species (Branda and Dymecki, 2004), their application is time and cost consuming. For example, it takes 4 weeks to construct a *LoxP* knockin line in *Caenorhabditis elegans* (Dickinson et al., 2013); and to produce a single gene conditional knockout, one must generate all of the necessary lines followed by another two generations of genetic crosses to produce homozygous experimental animals for phenotype analysis. Conditional knockouts of multiple genes require even more laborious intercrossing of single mutant animals and are not necessarily achievable if the target loci are tightly linked. RNA interference (RNAi) and temperature-sensitive (ts) alleles are another two principal methods to conditionally inactivate genes; however, their utility is limited by the variable penetrance of the phenotype due to the inherent incompleteness of protein inactivation or depletion (Pastrana, 2010). Moreover, RNAi may be accompanied by confounding off-target effects, and some types of *C. elegans* neurons are well known for being refractory to RNAi (Pastrana, 2010). Furthermore, it is not realistic to produce a ts allele of every gene in the genome. Thus, there remains a need for new conditional knockout technologies that are efficient, versatile, and easy to implement.

Recently, two classes of nucleases have been developed to introduce specific double-strand breaks (DSBs) at the desired genomic loci, rendering these nucleases as powerful tools for precise genomic engineering. Transcription activator-like effector nucleases (TALENs) bind as a pair around the target locus and introduce DSBs via a dimer of Fok I nuclease domains (Joung and Sander, 2013). The Cas9 nuclease from the clustered regularly interspaced short palindromic repeat (CRISPR)/CRISPR-associated (Cas) system is directed to a G(N)19NGG target genomic site by associating with a synthetic guide RNA (sgRNA) that hybridizes to a 17–20 nucleotide "protospacer" DNA sequence (Cong et al., 2013; Mali et al., 2013; Wiedenheft et al., 2012). The DSBs generated by TALENs or Cas9 nucleases are often erroneously repaired via nonhomologous end joining (NHEJ; Lieber, 2010), which is conducive to frameshift insertions or deletions (indels) that generate loss-of-function mutations of the target gene.

TALENs and the CRISPR-Cas9 system have been used in a wide range of species for genome editing. However, their application has largely been limited to cultured cells, embryos and the germline (Huang et al., 2011; Joung and Sander, 2013; Miller et al., 2011; Wood et al., 2011). The CRISPR-Cas9 system has recently been adapted for targeted genome modification in the *C. elegans* germline (Dickinson et al., 2013; Friedland et al.,

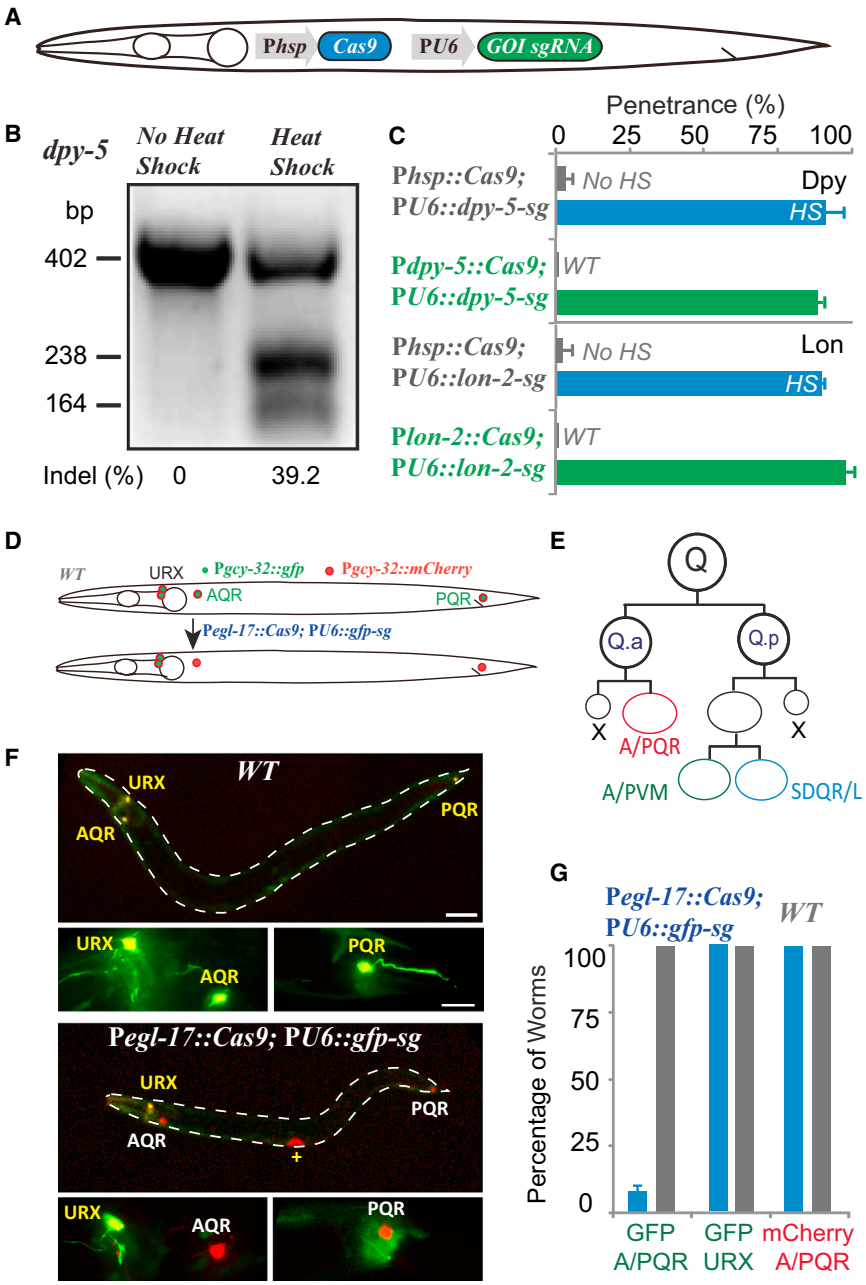

Figure 1. Conditional Mutation of *dpy-5*, *lon-2*, and *gfp* via the Spatiotemporally Regulated Expression of the CRISPR-Cas9 System in *C. elegans* Somatic Cell Lineages

(A) Schematic of the somatic CRISPR-Cas9 strategy for generating conditional knockouts in *C. elegans*. The plasmid that expresses Cas9 nuclease under the control of a heat-shock promoter (*Phsp*, gray) or a tissue-specific promoter (not shown) and an sgRNA corresponding to the gene of interest (GOI) under the control of the *U6* small nuclear RNA promoter was injected into the *C. elegans* germline.

(B) A representative gel of the T7EI assay for *dpy-5* PCR products amplified from the genomic DNA of worms expressing *Phsp::Cas9* and *PU6::dpy-5-sg* without (left) or with (right) heat-shock treatment.

(C) Upper: quantification of the Dpy phenotype in animals expressing the *Phsp::Cas9* and *PU6::dpy-5-sg* constructs without (gray) or with (blue, N = 142 from three independent experiments) heat-shock treatment 16 hr after egg-laying or in animals expressing *Pdpy-5::Cas9* and *PU6::dpy-5-sg* (green, N = 137 from three generations). "*dpy-5*-sg": the sgRNA targeting *dpy-5*. Lower: quantification of the Lon phenotype in animals expressing *Phsp::Cas9* (N = 212) or *Plon-2::Cas9* (N = 122) and *PU6::lon-2-sg*.

(D) Schematic of the use of the somatic CRISPR-Cas9 method to knockout *gfp* in *C. elegans* Q neuroblast lineages using the lineage-specific promoter *Pegl-17* to express Cas9. *Pgcy-32::gfp* and *Pgcy-32::mCherry* transgenes induce GFP (green) and mCherry (red) fluorescence, respectively, in URX, AQR, and PQR neurons.

(E) Schematic of the Q neuroblast lineages. Each QL or QR neuroblast generates three neurons and two apoptotic cells (Q.aa/Q.pp). QL produces PQR, PVM, and SDQL, and QR produces AQR, AVM, and SDQR.

(F) Fluorescence images of GFP (green) and mCherry (red) in URX and A/PQR in WT animals expressing *Pgcy-32::gfp* and *Pgcy-32::mCherry*, respectively (upper), or in worms expressing *Pegl-17::Cas9* and *PU6::gfp-sg* (lower) under a 10× objective (each upper image, scale bar represents 50 μm) or a 100× objective (lower two images, scale bar represents 5 μm). +, vulva.

(G) Quantification of the GFP- or mCherry-positive URX and A/PQR neurons in WT worms (gray) or in worms expressing *Pegl-17::Cas9* and *PU6::gfp-sg* (blue, N = 138 from three generations). The error bars indicate SD.

See also Figure S1.

2013; Frøkjær-Jensen, 2013). Here, we report that conditional knockout can be achieved in *C. elegans* somatic cell lineages by expressing the CRISPR-Cas9 system with an inducible or tissue-specific promoter (hereafter referred to as somatic CRISPR-Cas9). We show that this platform facilitates the production of conditional knockouts in various cell types or in multiple genomic regions in one step. Via live cell imaging analysis of neuroblast development in conditional knockout animals, we examined the function of a homolog of the embryonically essential protein Coronin in postembryonic neural migration and neuritogenesis in *C. elegans*.

RESULTS

Somatic Utilization of the CRISPR-Cas9 System Induces Conditional Targeted Genomic Mutations in *C. elegans*

To establish somatic CRISPR-Cas9 as a general tool for conditional genome editing in *C. elegans*, we first generated transgenic animals that specifically express the Cas9 nuclease in somatic cell lineages under the control of a heat-shock-inducible promoter or a tissue-specific promoter and that ubiquitously express the sgRNA under the control of the *U6* promoter (Figure 1A; see also Protocol available online). As proof-of-principle

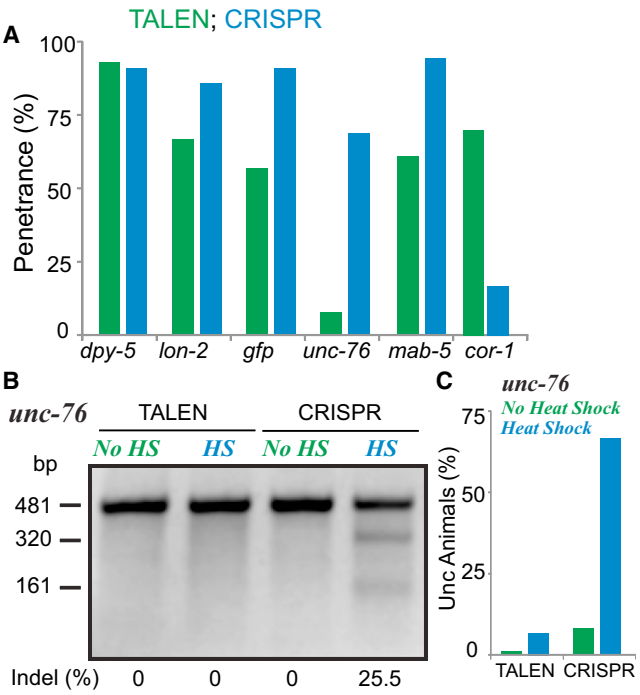

Figure 2. Comparison of the Efficiency between Somatic TALENs and Somatic CRISPR-Cas9

(A) The penetrance of the phenotypes corresponding to the *dpy-5*, *lon-2*, *gfp*, *unc-76, mab-5*, and *cor-1* conditional mutant animals using somatic TALENs (green) or somatic CRISPR-Cas9 strategy (blue) to target the same site. The somatic TALEN data for *dpy-5*, *lon-2*, *gfp*, and *mab-5* were derived from a previous study (Cheng et al., 2013).

(B) A T7EI assay gel comparing the *unc-76* mutation efficiency between somatic TALENs and somatic CRISPR-Cas9. HS, heat-shock induction.

(C) Quantification of the Unc phenotype in animals expressing the P*hsp::unc-76*-TALENs (TLR) constructs (N = 126) or expressing P*hsp::Cas9* and P*U6::unc-76-sg* (N = 127).

See also Figure S2 and Movies S1 and S2.

experiments, we designed sgRNAs complementary to the coding sequences of *dpy-5* and *lon-2*, both of which are expressed in the *C. elegans* epithelium and regulate body length (Gumienny et al., 2007; Thacker et al., 2006). We chose these genes for targeting because their null mutant alleles cause easily identifiable dumpy (Dpy) or long (Lon) phenotypes, respectively. We hypothesized that indels generated using the CRISPR-Cas9 system in somatic cells would mimic these defects.

To achieve the temporally regulated mutation of *dpy-5* or *lon-2*, we expressed Cas9 nuclease under the heat-shock gene *hsp-16.2* promoter P*hsp* (Figures 1B and 1C). We generated transgenic animals by injecting a plasmid containing both Cas9 and sgRNA, along with a selection marker, into the *C. elegans* germline (Mello et al., 1991). In transgenic animals, the sgRNA targeting *dpy-5* or *lon-2* was referred to as *dpy-5-sg* or *lon-2-sg*, respectively. After heat-shock treatment of L1 larvae, we detected the Dpy or Lon phenotype in the adult transgenic animals with the penetrance of 91% ± 6% (mean ± SD, N = 142 for *dpy-5*) and 86% ± 1% (N = 212 for *lon-2*), respectively (Figures 1C; Figures S1A, S1D, and S2; data from three generations). We found that the Dpy penetrance increased in the late embryos, when the P*hsp* was activated (Stringham et al., 1992), peaking at the L1 larval stage when treated with heat shock because *dpy-5* begins to function at this stage (Thacker et al., 2006; Figure S1B). Neither the Dpy nor Lon phenotype was observed in transgenic animals not subjected to heat shock (Figure 1C, N = 304 for *dpy-5-sg*, N = 151 for *lon-2-sg*). To produce a spatially controlled *dpy-5* or *lon-2* mutant, we expressed Cas9 using the endogenous promoter of *dpy-5* or *lon-2* (P*dpy-5* or P*lon-2*). We showed that transgenic animals exhibited the Dpy (87% ± 2% for *dpy-5-sg*, N = 137) or Lon phenotype (98% ± 3% for *lon-2-sg*, N = 122), respectively (Figures 1C and S2).

Because DSBs are partially repaired by the NHEJ pathway, we performed the T7EI assay (Cong et al., 2013) to detect the indels produced by *dpy-5-sg*. We PCR-amplified a genomic 402-bp DNA fragment containing the target site from *dpy-5-sg* transgenic animals. After T7EI digestion, the PCR fragment from the transgenic animals treated with heat shock was cut into two small fragments but remained intact in the animals not subjected to heat shock (Figure 1B). Sanger sequencing of these PCR amplicons confirmed that short insertions and deletions had indeed occurred at the target *dpy-5* site (Figure S1C). For the *lon-2* locus, we detected small indels as well as large deletions (more than 100 bp; Figure S1E), indicating that the NHEJ pathway may repair specific loci in a different manner.

To extend our initial results on *dpy-5* and *lon-2* to the nervous system, we determined the feasibility of using somatic CRISPR-Cas9 to conditionally knockout multiple copies of a *gfp* transgene in *C. elegans* Q neuroblast lineages. We used the P*gcy-32* promoter to express *gfp* in URX, AQR, and PQR neurons (A/PQR; Figures 1D and 1E). Because germline microinjection and subsequent integration into *C. elegans* insert many copies of the transformed DNA into its genome (Mello et al., 1991), the GFP fluorescence of P*gcy-32::gfp* is detectable in these neurons at low magnification (Figure 1F). In these animals, we expressed Cas9 under the control of the Q neuroblasts-specific P*egl-17* promoter and the sgRNA complementary to *gfp* under the control of the P*U6* promoter. As A/PQR neurons, but not URX neurons, are derived from Q neuroblast lineages (Figure 1E), the GFP fluorescence was specifically disrupted in A/PQR neurons of 91% ± 2% of the transgenic animals (N = 137). We did not find any loss of GFP fluorescence in URX neurons, nor did we detect the loss of red fluorescence from the P*gcy-32::mCherry* reporter (N = 137, Figures 1F and 1G). These results demonstrate that the somatic CRISPR-Cas9 method efficiently knocks out multiple copies of a transgene in specific cell lineages.

Somatic CRISPR-Cas9 Outperforms Somatic TALENs across Most Loci

Previously, we used somatically expressed TALENs as an effective tool to generate conditional knockouts in *C. elegans* (Cheng et al., 2013). We compared the relative efficacies of somatic CRISPR-Cas9 and somatic TALENs in mutating the same genomic sites. Somatic TALEN experiments successfully targeted *dpy-5*, *lon-2*, *gfp*, *mab-5*, and *cor-1* at efficiencies of 51%–91% (Figure 2A; Cheng et al., 2013). Using the same delivery platform, somatic CRISPR-Cas9 yielded conditional mutations of all of these loci (Figure 2A). Except for the *cor-1* gene, the mutation efficiency ranged from 86% to 97%, indicating

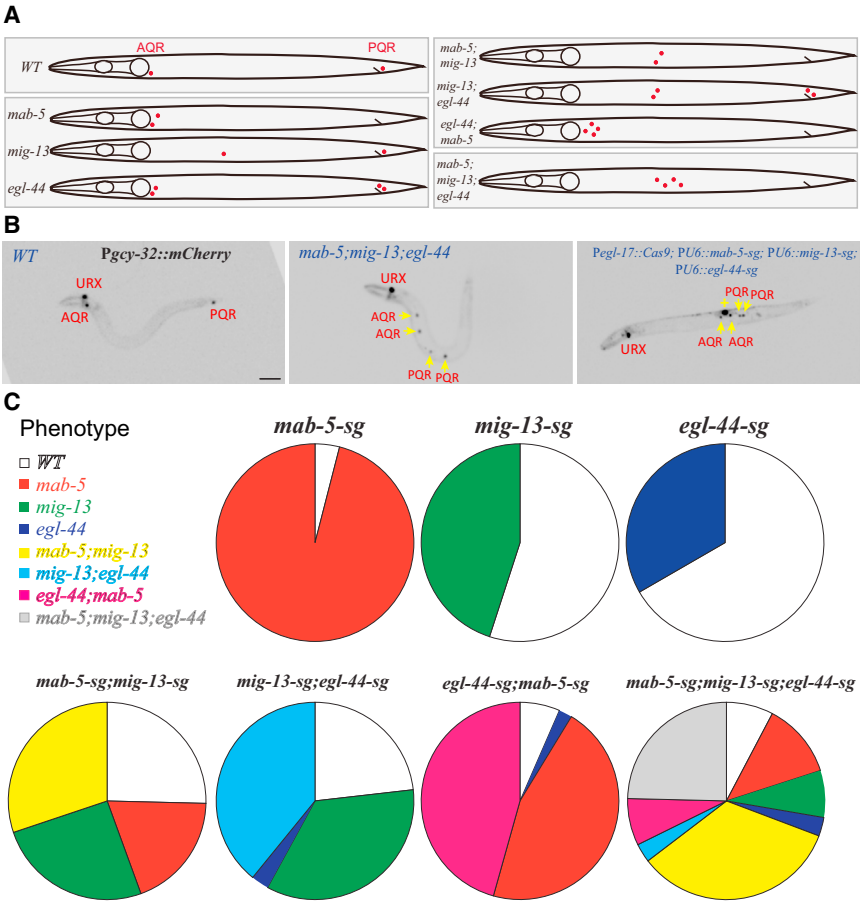

Figure 3. One-Step Generation of Multiple Conditional Knockouts of *mab-5*, *mig-13*, and *egl-44* in *C. elegans* Q Neuroblast Lineages

(A) Schematics of the A/PQR position and number in WT and *mab-5*, *mig-13*, and *egl-44* single, double, or triple mutant animals. Fluorescence images of the A/PQR neurons in the WT and mutant animals and the penetrance of the corresponding phenotypes are shown in Figures S3 and S4.

(B) Inverted images of the A/PQR position and number in the WT (left), *mab-5*; *mig-13*; *egl-44* triple mutant (middle), and CRISPR-Cas9 construct-expressing transgenic animals to conditionally knock out these three genes (right). A/PQR neurons are demonstrated using P*gcy-32::mCherry*. The image is inverted so that high mCherry fluorescence intensity is black. The cell identities are denoted adjacent to the cells. The yellow arrows indicate an A/PQR neuron displaying a defect in cell migration or cell cycle exit. +, vulva. Scale bar represents 50 μm. Images of the single and double conditional knockouts are in Figure S3.

(C) Quantification of the A/PQR migration and cell division phenotypes in the single, double, and triple conditional knockout animals. The genotypes are indicated above the graph (N = 46–69). See also Figure S3.

that somatic CRISPR-Cas9 is more efficient than (*lon-2*, *gfp*, and *mab-5*) or equivalent to (*dpy-5*) somatic TALENs (Figure 2A).

Next, we explored the potential for somatic CRISPR-Cas9 to produce conditional mutations at a locus that was not efficiently targeted using somatic TALENs. Our attempt to conditionally mutate *unc-76*, which is crucial for axonal outgrowth and fasciculation (Bloom and Horvitz, 1997), was not successful when using heat-shock-induced TALENs; the T7EI assay did not detect molecular lesions, and the uncoordinated (Unc) phenotype was barely detectable after heat shock (N = 104; Figures 2B and 2C). In contrast, using somatic CRISPR-Cas9 method to target the same site in *unc-76* produced indels at the target site and the Unc behavioral defect in 69% ± 1% of the transgenic animals (N = 127; Figures 2B, 2C, and S2; Movies S1 and S2), indicating that somatic CRISPR-Cas9 conditionally mutated a gene that could not be modified using somatic TALENs. Comparing these data directly, the somatic CRISPR-Cas9 technique improves the efficiency of conditional knockout across most loci.

One-Step Generation of Double- and Triple-Gene Conditional Knockouts using Somatic CRISPR-Cas9

A rapid and multipliable conditional knockout approach is critical for dissecting the redundant functions of gene family members and for analyzing genetic relationships in specific cell types or at distinct developmental stages. Because mutations generated using the somatic CRISPR-Cas9 method are often hypomorphic, care must be taken if such mutations are used for epistatic analysis, as the results may not be informative. However, these mutations can be used for epistatic analysis if they are in the epistatic loci. In *C. elegans*, a mixture of different DNA molecules can be coinjected and coinherited via extrachromosomal arrays across generations (Mello et al., 1991). We explored whether double- or triple-gene conditional knockouts can be generated in one step by coinjecting plasmids that express multiple sgRNAs targeting different genes.

To examine this possibility, we selected three genes to generate conditional mutations based on their well-characterized function in Q neuroblast migration or division. In wild-type (WT) animals, the bilateral QL and QR neuroblasts on the left and right sides of *C. elegans* undergo three rounds of asymmetric cell division, producing cells that migrate in the opposite direction along the anterioposterior body axis (Sulston and Horvitz, 1977). A homeodomain transcription factor (TF), *mab-5*, regulates the direction of QL.x (QL descendant) migration, and its loss of function mutation converts PQR posterior migration to the anterior direction (Kenyon, 1986); *mig-13*, a transmembrane protein, regulates QR.x migration, and its null mutation reduces AQR anterior migration (Wang et al., 2013); and *egl-44*, a TEA domain TF, mediates cell cycle exit, and its mutation produces additional A/PQR neurons (Feng et al., 2013; Figure 3A). MAB-5, MIG-13, and EGL-44 act independently via three distinct regulatory pathways, and we showed that their additive phenotypes were easily evaluated in the double or triple mutants (Figures 3A, S3A, and S3B).

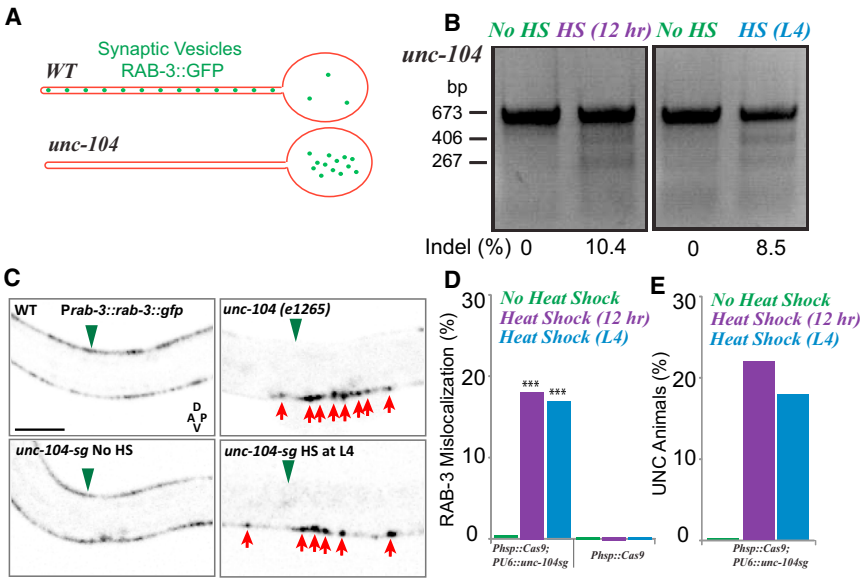

Figure 4. The Somatic CRISPR-Cas9 Strategy Generates Conditional Knockouts in *C. elegans* Postmitotic Neurons

(A) Schematic showing that *unc-104* (kinesin-3) delivers synaptic vesicles from the soma to the axon.

(B) T7EI assay showing the cleavage efficiency of the *unc-104* gene conditionally mutated in animals expressing P*hsp::Cas9* and P*U6::unc-104-sg* at 12 hr after egg-laying or at the L4 larval stage.

(C) Inverted fluorescence images of synaptic vesicles labeled with RAB-3::GFP in *C. elegans* motor neurons in WT, *unc-104*, and *unc-104-sg* animals. The red arrows indicate the accumulation of RAB-3::GFP in the ventral nerve cord; the green arrows indicate the dorsal nerve cord. Scale bar represents 5 μm.

(D and E) Quantification of the mislocalization of RAB-3::GFP (D, N = 21–53) and the Unc phenotype in *unc-104-sg* animals (E, N = 35–71). Statistical significance: ***p < 0.001 based on the chi-square test.

See also Movies S3 and S4.

We constructed Cas9-sgRNA plasmids that specifically express Cas9 in Q neuroblast lineages and ubiquitously express sgRNA targeting *mab-5*, *mig-13*, or *egl-44*. We injected each plasmid into the *C. elegans* gonad, and we showed that the transgenic animals displayed the expected molecular lesion at each target site (Figure S3C). We detected the single-mutant phenotypes at a penetrance of 97% (anterior PQR migration in *mab-5-sg*), 45% (reduced AQR migration in *mig-13-sg*), and 33% (additional A/PQR neurons in *egl-44-sg*; Figures 3B, 3C, and S3A). Next, we coinjected two plasmids targeting two genes and observed the predicted double-mutant phenotypes in transgenic animals: 30% of the *mab-5-sg* and *mig-13-sg* coinjected animals exhibited reduced anterior migration of both the AQR and PQR neurons; 46% of the *mab-5-sg* and *egl-44-sg* coinjected animals generated two PQR neurons that moved anteriorly; and 39% of the *egl-44-sg* and *mig-13-sg* coinjected animals produced two AQR neurons that displayed reduced anterior migration (Figures 3B, 3C, and S3A). Notably, after we cotransformed the three plasmids targeting all the three genes, we found that 24% of the transgenic animals exhibited the three additive defects, the PQR migration direction, the AQR migration distance, and the A/PQR number (Figures 3B and 3C). The defects observed in the conditional knockout transgenic animals were indistinguishable from those in the double- or triple-mutant animals, regardless of the lower penetrance of the phenotypes than that of the genetic mutants (Figures S3A and S3B). We conclude that one-step microinjection efficiently generates multiple conditional knockouts within a single transgenic animal. Interestingly, we found that the cell migration defect in the *mig-13* single mutants was enhanced in the *mig-13; egl-44* double conditional knockouts (Figure 3C), and we confirmed the increased penetrance in the *mig-13; egl-44* double genetic mutants (Figure S3B). These results suggest that *egl-44* may function in parallel with *mig-13* to regulate cell migration, even though the *egl-44* single mutation does not affect cell migration.

Somatic CRISPR-Cas9 Conditionally Mutates Genes in Postmitotic Cells

The molecular dissection of the physiology of postmitotic cells requires gene inactivation after mitosis. Therefore, we sought to generate conditional knockouts in postmitotic neurons using somatic CRISPR-Cas9. We chose to conditionally mutate *unc-104*, which encodes a kinesin-3 family motor protein essential for axonal transport of synaptic vesicles in mature neurons (Figure 4A; Hall and Hedgecock, 1991). We constructed transgenic animals that express Cas9 under the control of P*hsp* and sgRNA targeting the *unc-104* site under the control of P*U6*. Because the final somatic cell divisions in *C. elegans* (the epithelial seam cells) occur at the early L4 larval stage (Sulston and Horvitz, 1977), we induced Cas9 expression by treating L4 transgenic larvae with heat shock, and the T7EI assay detected indels at the *unc-104* locus (Figure 4B). To compare the localization of synaptic vesicles among the WT, *unc-104*, and *unc-104-sg* animals, we visualized synaptic vesicles using a GFP-tagged RAB-3 marker in *C. elegans* DA motor neurons (Nonet et al., 1997), whose cell bodies are located in the ventral nerve cord and whose axonal commissures extend to the dorsal nerve cord (Figure 4C). In the WT animals and the *unc-104-sg* transgenic animals not subjected to heat shock, RAB-3::GFP fluorescence was evenly distributed along the dorsal and ventral nerve cord. However, in the *unc-104* mutants and the *unc-104-sg* animals treated with heat shock (18%, N = 65), RAB-3::GFP fluorescence was absent from the axonal commissures in the dorsal nerve cord but accumulated in the cell bodies in the ventral nerve cord, indicating that the synaptic vesicles were not delivered to the axons (Figures 4C and 4D). We did not detect any defect in the distribution of RAB-3::GFP in P*hsp::Cas9* transgenic animals treated with heat shock (Figure 4D). Furthermore, we found that 18% of the *unc-104-sg* animals developed the Unc phenotype after heat shock (N = 175, Figure 4E; Movies S3 and S4). These molecular, cellular, and behavioral results indicated that somatic CRISPR-Cas9 efficiently mutated *unc-104* after mitosis.

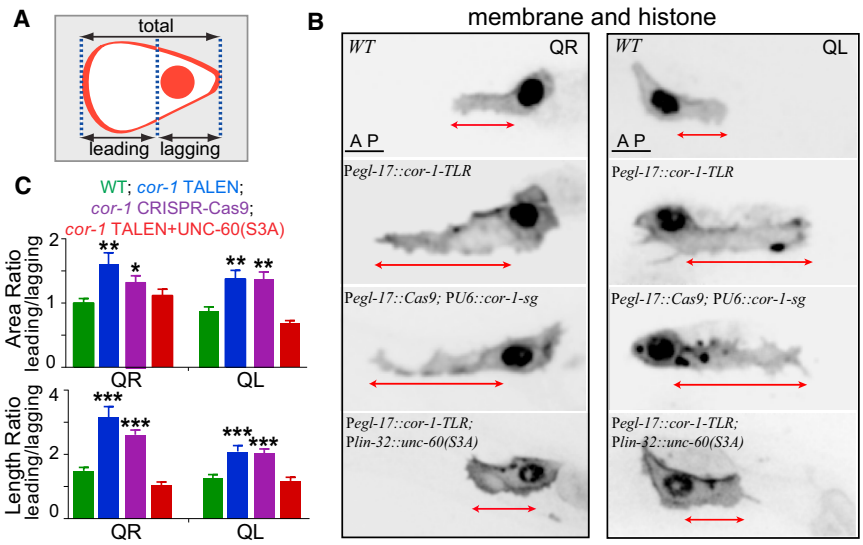

Figure 5. Live Imaging Analysis of *cor-1* Conditional Knockouts Revealed Its Role in Regulating Cell Morphology during Q Neuroblast Migration

(A) Schematic of a migrating Q cell. The anterior, posterior, and total length or area of the Q cell was quantified as indicated.

(B) Inverted fluorescence images of the QR (left) and QL cell (right) morphology in the WT and *cor-1* conditional knockout animals. The Q-cell membrane and histones are labeled with mCherry. The double-headed arrows indicate the leading area (from the front of the nucleus to the leading edge). The genotypes are indicated on the top left; TLR, TALEN. Anterior, left. Scale bar represents 5 μm.

(C) Quantification of the area (upper) and length (lower) ratios of the leading end to the lagging end of Q neuroblasts in the WT and *cor-1* conditional knockout animals (N = 10–27). The error bars indicate SEM. Statistical significance: *p < 0.05; **p < 0.01; ***p < 0.001 based on Student's t test. See also Figure S4.

To expand our initial results to other neuron types, we chose to target two additional loci, *unc-76* and *gfp*. Using the heat-shock strategy described above, the T7EI assay showed that somatic CRISPR-Cas9 conditionally generated indels at the *unc-76* site in L4 larvae (Figure S3C). In addition, we found that 10% of the *unc-76-sg* animals (N = 121) developed the Unc phenotype, the penetrance of which was lower than that of treatment of the embryos with heat shock, because *unc-76* regulates early neural development in *C. elegans* (Bloom and Horvitz, 1997). Next, we examined whether Cas9 expression driven by P*mec-7* or P*gcy-32*, which become activated after the birth of neurons from Q cell lineages, generates conditional knockouts of multiple copies of the *gfp* gene. We transformed plasmids expressing Cas9 and *gfp*-targeted sgRNA into strains stably expressing the reporter P*mec-7::gfp* or P*gcy-32::gfp* in mechanosensory or oxygen-sensory neurons. Because both reporters are integrated into the genome, the GFP fluorescence is visible in these neurons in all of the animals (N > 100 for each). However, the GFP fluorescence was absent from 49 of the 61 P*mec-7::Cas9; PU6::gfp-sg* transgenic animals and 93 of the 118 P*gcy-32::Cas9; PU6::gfp-sg* transgenic animals, further indicating that the somatic CRISPR-Cas9 strategy enables conditional gene disruptions in postmitotic neurons.

Live Imaging of Conditional Knockouts Revealed the Roles of Coronin in Neural Development

We performed live imaging analysis of *C. elegans* conditional knockout animals to determine the function of an essential embryonic gene in postembryonic neuroblast development. By creating a conditional knockout using somatic CRISPR-Cas9 or TALENs, we bypassed the embryonic requirement for *cor-1*, a worm Coronin homolog that is associated with human neurobehavioral disabilities (Jayachandran et al., 2014) and severe combined immunodeficiency (Shiow et al., 2008), and examined its function in neural development. Previous studies using cell lines indicated that Coronin, an actin binding protein, promotes the disassembly of actin filaments (Cai et al., 2007, 2008; Chan et al., 2011), but the cellular mechanisms of Coronin function in animal models are controversial. Mouse genetics revealed that Coronin 1 regulates T cell chemotaxis and homing to lymph nodes by modulating actin dynamics (Föger et al., 2006), whereas another study implied that Coronin 1 regulates T cell viability independent of the actin cytoskeleton by modulating calcium signaling (Mueller et al., 2011). In the nervous system, Coronin 1 has been demonstrated to modulate cyclic AMP/PKA-dependent synaptic plasticity (Jayachandran et al., 2014) or mediate NGF-TrkA endosome stability, recycling, and signaling to promote neuronal survival (Suo et al., 2014). Our recent study using somatic TALENs showed that *cor-1* specifically regulates Q-cell migration but is dispensable for Q cell division, survival or apoptosis (Cheng et al., 2013). To exclude the possibility of the off-target cleavage of TALENs at the *cor-1* locus, we used the somatic CRISPR-Cas9 method to further examine the role of COR-1 in Q cell development. We generated transgenic animals expressing Cas9 in Q cell lineages and sgRNA targeting the *cor-1* gene, and we showed that 13% of the AQR neurons and 16% of the PQR neurons (N = 30) displayed a reduced migration distance (Figure S4A). We did not detect any other defects in Q cell development in the *cor-1* conditional mutants. These results reinforced our previous finding that COR-1 plays a specific role in *C. elegans* Q neuroblast migration.

We addressed the mechanism by which COR-1 regulates Q cell migration by examining Q cell morphology in WT and *cor-1* conditional knockout animals. In this experiment, we imaged the Q cell membrane and nucleus using mCherry tagged with a myristoylation signal and a histone. During Q cell migration in WT animals, the QR or QL neuroblast elongates toward its direction of migration and extends a lamellipodium with a modest size. By measuring ratio of the area or the length of the leading to lagging portions of the Q neuroblasts, we showed that these ratios were approximately equal (Figures 5A–5C and S4B). Strikingly, in *cor-1* conditional knockouts generated using the somatic TALENs or somatic CRISPR-Cas9 strategy, the Q cell morphology was dramatically altered, including the formation of oversized larger leading area (Figures 5B, 5C, and S4B). We found that the size and the length ratios in the *cor-1* conditional

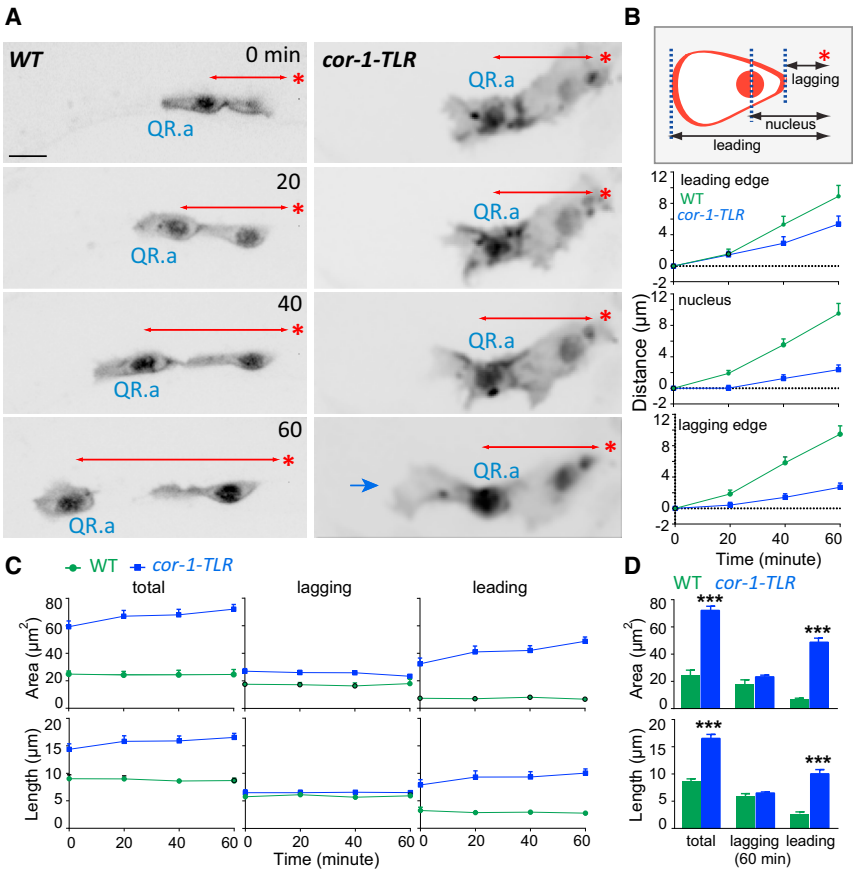

Figure 6. Time-Lapse Analysis of QR.a Cell Migration in the *cor-1* Conditional Mutants

(A) Inverted fluorescence images of QR.a cell morphology in the WT (left) and *cor-1* conditional knockout (right) animals. The Q cell membrane and histones are labeled with mCherry. The double-headed arrows indicate the distance from the center of the Q cell nucleus to a fiducial marker (asterisk). A nonmotile autofluorescence particle adjacent to the migrating cell was chosen as the fiducial marker. Scale bar represents 5 μm.

(B) Quantification of the distance from the leading edge, the nucleus, or the lagging edge of the Q cell to the fiducial marker in the WT (N = 9) and *cor-1* conditional mutant animals (N = 12). A schematic of the measurement is at the top.

(C) Quantification of the change in the area or length of the QR.a cell during migration in the WT (N = 9) and *cor-1* conditional mutant animals (N = 12).

(D) Statistical analysis of the area or length of the QR.a cell 60 min after migration in the WT (N = 9) and *cor-1* conditional mutant animals (N = 12). The error bars indicate SEM. Statistical significance: ***$p < 0.001$ based on Student's t test.

See also Figure S5 and Movies S5 and S6.

mutants were from 1.3- to 1.6-fold larger and from 1.6- to 2.1-fold longer than those in WT cells, respectively (Figures 5C and S4B).

To understand the mechanism by which Q cells develop an abnormally large leading area in the *cor-1* conditional knockout animals, we performed live imaging analysis of the migrating QR.a cell using an integrated *C. elegans* strain that stably expresses somatic TALENs mutating *cor-1*. In contrast to the consistent translocation of the leading edge, the nucleus, and the lagging edge of QR.a in the WT animals, QR.a in *cor-1* conditional knockouts continuously extends its leading edge but leaves its nucleus and lagging edge behind (Figures 6A and 6B). Consequently, the size and length of the anterior area gradually increase, whereas those of the posterior area do not change during migration (Figures 6A, 6C, and 6D; Movies S5 and S6). We observed similar migration and cellular defects in QR.ap of the *cor-1* conditional knockouts (Figure S5).

To dissect the molecular pathway involved in establishing the appropriate cell morphology, we examined the F-actin distribution in migrating Q cells using an in vivo F-actin probe, the actin-binding domain of moesin (GFP::moesinABD; Chia et al., 2014). When expressed in Q cells, GFP::moesinABD is enriched in the leading edge, and the GFP intensity in the anterior area is 1.8-fold (QR.a) or 2.3-fold (QR.ap) higher than that in the posterior area (Figures 7A, S4C, and S4D). In the *cor-1* conditional knockouts, ectopic actin bundles (longer than 2 μm) assemble behind the leading edge, and the GFP fluorescence of GFP::moesinABD accumulates in the lagging area, causing an even distribution of F-actin in QR.a and QR.ap (Figures 7B, 7C, S4C, and S4D; Movies S7 and S8). These defects in F-actin distribution indicated that Coronin regulates neuroblast migration by coordinating the organization of the actin cytoskeleton.

Next, we examined the mechanism underlying ectopic F-actin assembly in migrating cells in which Coronin expression is depleted. In vitro biochemical analysis revealed that Coronin recruits the phosphatase Slingshot to lamellipodia, where Slingshot activates Cofilin via dephosphorylation (Cai et al., 2007). Accordingly, Coronin promotes the phospho-Cofilin levels, and inactivation of Coronin reduces the activity of Cofilin. We examined whether ectopic F-actin formation partially results from the inactivation of Cofilin during Q cell migration. UNC-60, the worm homolog of human Cofilin (displaying 31% amino-acid sequence identity and 50% sequence similarity), contains a highly conserved Serine 3, whose dephosphorylation enhances the severing activity of Cofilin to on F-actin (Cai et al., 2007). To address this issue, we expressed an activated Cofilin/UNC-60 mutant (S3A) in *cor-1* conditional knockouts, and we found that Cofilin (Figure S3A) significantly reduced the size and the length of the leading area to levels similar to those observed in WT cells (Figures 5B and 5C). To examine F-actin distribution, we introduced the GFP::ABDmoesin marker into the *cor-1* conditional knockouts expressing Cofilin (Figure S3A). We showed that the ectopic long actin filaments were significantly absent from the QR, QR.a and QR.ap cells (Figures 7C and S4C). Our results suggest that the role of Coronin in actin filament turnover via Cofilin is essential for determining cell morphology during Q cell migration. As reported previously, Cofilin S3A rescued the lamellipodial dynamics associated with the depletion of Coronin but did not rescue the defects in the whole-cell motility of fibroblasts (Cai et al., 2007); and we did not observe that Cofilin S3A transgenes suppress the *cor-1* migration defects either (data

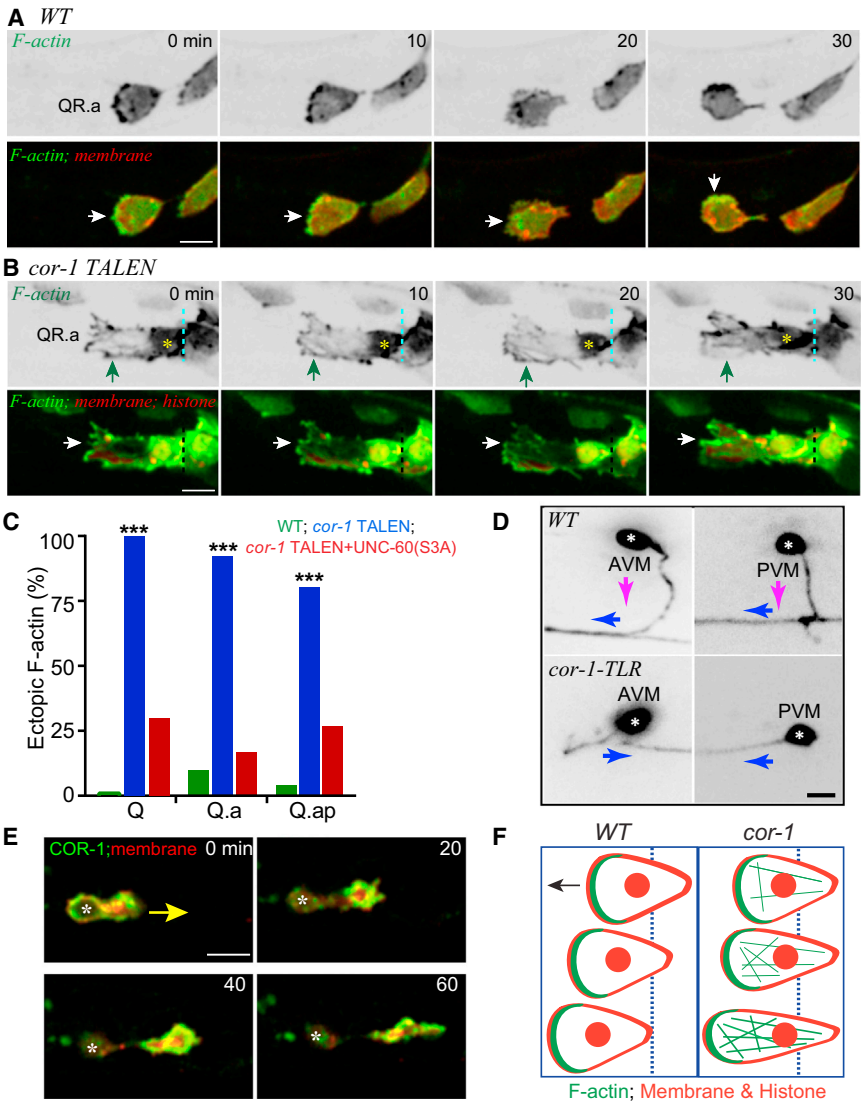

Figure 7. Actin Cytoskeleton Formation and Neuritogenesis in Q Neuroblasts of *cor-1* Conditional Mutants

(A and B) Fluorescence time-lapse images of F-actin (GFP:: ABDmoesin) in the QR.a cell of WT (A) and *cor-1* conditional knockout (B) animals. The white arrows indicate the leading edge; the green arrows (B) indicate long F-actin; and the asterisks indicate the lagging area (B). The GFP image (upper) is inverted, and the merged images are in the lower images. The dotted lines (B) indicate the lagging edge. Scale bar represents 5 μm.

(C) Quantification of the formation of ectopic actin filaments (longer than 2 μm) in Q neuroblasts of WT and *cor-1* conditional mutant animals (N = 9–27). Statistical significance: ***p < 0.001 based on the chi-square test.

(D) Neurites of the AVM (left) and PVM (right) neurons in the WT (upper) and *cor-1* conditional mutant animals (lower). The pink and blue arrows indicate dorsal-ventral and anterior-posterior growth of the neurites, respectively. Asterisk, cell body. Scale bar represents 5 μm.

(E) The merged images show that COR-1::GFP localizes to the QL.ap cell growth cone. The yellow arrow indicates the growth direction of the QL.ap cell growth cone. The asterisks denote the soma.

(F) A proposed model of the roles of COR-1 in regulating actin organization and cell morphology during Q cell migration.

See also Figure S4 and Movies S7, S8, and S9.

not shown), suggesting that another function of Coronin, such as its inhibition of Arp2/3 complex-mediated actin nucleation, may be crucial for cell migration. We propose that the loss-of-function of Coronin promotes the assembly of actin monomers into long actin bundles, which depletes the actin monomer pool that is necessary for continued actin assembly at the leading edge of migrating neuroblasts (Figure 7F).

DISCUSSION

We described an inducible strategy to express the CRISPR-Cas9 system as an effective means of introducing conditional mutations to various somatic cell types of *C. elegans* at different developmental stages. Our study demonstrates that the somatic CRISPR-Cas9 platform facilitates the study of cell migration (*mab-5*, *mig-13* and *cor-1*), cell division (*egl-44*), neuritogenesis (*unc-76*), axonal transport (*unc-104*), and epithelial development (*dpy-5* and *lon-2*), rendering somatic CRISPR-Cas9 as a versatile tool to address cellular and developmental questions in live animals.

The Somatic CRISPR-Cas9 Technique for Generation of Conditional Knockouts

The somatic CRISPR-Cas9 platform provides advantages over other conditional knockout techniques. Somatic CRISPR-Cas9 enables the most rapid production of conditional knockouts. This strategy facilitates the analysis of conditional knockout phenotypes in the F1 generation of transgenic animals, requiring only 1 week total time beginning from the experimental design in *C. elegans*. The hands-on time can be as little as 3 hr: 2 hr for plasmid construction and 1 hr for transgene microinjection. Moreover, the somatic CRISPR-Cas9 technology produces multiple conditional knockouts in one step at the same cost of time and effort as performing a single conditional mutation, irrespective of the genetic positions of the target loci. Our studies broaden the repertoire of multiple genome modifications in mammalian cell lines or embryos via the delivery of multiple sgRNAs (Cong et al., 2013; Yang et al., 2013). Because transgenic DNA as large as yeast artificial chromosomes can be used for *C. elegans* germline transformation (Mello et al., 1991), conditional knockouts of more than three loci may be produced simultaneously by introducing pooled plasmids targeting multiple genes. The application of somatic CRISPR-Cas9 is easier than that of somatic TALENs because the Cas9 nuclease is fixed in this system and because sgRNA construction requires only a simple swap of the 19-nucleotide protospacer, whereas each TALEN pair must be constructed de novo. Together, the

somatic CRISPR-Cas9 strategy is more rapid, versatile, and cost-effective than other conditional knockout techniques.

Despite these advantages, some potential limitations are associated with the use of the somatic CRISRP-Cas9 method. First, the molecular lesions induced by somatic CRISPR-Cas9 are heterogeneous, in contrast to the Cre/*Lox*P system, for which the structure of the conditional deletion is precisely known. Second, the efficiency of somatic CRISPR-Cas9 is variable across loci. Nine genes were targeted in this study; some of the phenotypes were induced at an efficiency that was higher than 90% (e.g., *dpy-5, lon-2, gfp*, and *mab-5*), but for other phenotypes, the induction efficiency was in the range of 10%–20% (e.g., *cor-1*). Because the CRISPR-Cas9 technology is under development, the basis of this variation in its efficiency is poorly understood. One explanation could be that the chromatin accessibility of the target site is thought to be crucial for the binding of Cas9 to the DNA (Wu et al., 2014). From a practical standpoint, the examination of different sites in a target gene may aid in the identification of the most efficient target sequence (Zhou et al., 2014). Another strategy to improve this efficiency is to screen for the best strains from multiple transgenic lines. Because the *C. elegans* extrachromosomal transgene is unique to some extent in each transgenic strain, we detected variations in the efficiency between the transgenic lines expressing the same target construct. Thus, we screened at least five independent lines whose transmission rates were greater than 50% and selected the two lines displaying the highest efficiency for further analysis. As long as the transgenic line is established, the penetrance of the phenotype is reproducible across generations (Figure S2). Given that the construction of the CRISPR-Cas9 plasmids and the injection of the transgenes into WT germlines are straightforward processes, the selection of multiple target sites or transgenic lines may be a useful solution to achieve the highest possible efficiency.

Our results regarding *cor-1* provide an example that the combination of the somatic CRISPR-Cas9 and somatic TALEN approaches may alleviate the concern of off-target effects. Because the binding of Cas9 or TALEN to the target genomic DNA sequence is individually guided by the base-pair complementarities or the interaction between variable residues in the TALE repeat and the DNA base (Cong et al., 2013; Mali et al., 2013; Miller et al., 2011), the confirmatory results obtained using somatic CRISPR-Cas9 and somatic TALEN approaches may suggest the actual function of the target gene. In this study, we targeted eight additional genes but did not detect other discernible phenotypes, nor did we detect any off-target mutations in our earlier study that used somatic TALENs (Cheng et al., 2013).

To elucidate the function of a gene for which the phenotype is not known in advance, mutant animals carrying a deletion in the target gene can initially be used to examine the phenotype. If there is no defect, the somatic CRISPR-Cas9 technique would not be advisable for studying this gene, because the target gene may not be essential or may perform a redundant function with other genes. The somatic CRISPR-Cas9 method, similar to other conditional knockout approaches, is valuable for elucidating functions of embryonically lethal genes. In these studies, we can initially validate the functionality of the sgRNA sequence by examining the embryonic lethality phenotype using P*hsp*::Cas9 animals and T7EI assays. If there is a novel phenotype, it must be confirmed by mutating additional sites in the gene, and if no defect is observed, caution must still be taken in the interpretation of these negative results. In either case, other conditional knockout methods can help to verify the findings.

The somatic CRISPR-Cas9, somatic TALENs, Cre/*LoxP*, and FLP/*FRT* technique are complementary tools to generate conditional knockout animals. The CRISPR-Cas9 system yields higher mutation efficiencies than TALENs for most loci across species (Ding et al., 2013), but the somatic TALEN method is more efficient at the *cor-1* site (Figure 2A), indicating that the TALEN method may provide an alternative approach to modify a locus that is challenging for the somatic CRISPR-Cas9 method. Although the mutations produced by somatic CRISPR-Cas9 or somatic TALENs are not heritable, indels generated via the NHEJ pathway caused frameshifts of the open reading frames in target genes (e.g., 90% of the indels on *dpy-5*, N = 10, Figure S1C; or 73% of the indels on *lon-2*, N = 11, Figure S1E). Given that the CRISPR-Cas9 cleavage sites are located in the first (*dpy-5*) or second exon (*lon-2*), these indels may generate strong loss-of-function mutations in the target genes. Consistently, we observed the constant penetrance of diverse conditional phenotypes across loci across generations (Figure S2). However, if an identical mutation is required, the Cre/*LoxP* or FLP/*FRT* system should be used. Thus, somatic CRISPR-Cas9 can initially be used to quickly assess the conditional knockout phenotype; the somatic TALEN method can be applied in further confirmatory trials; and finally, the Cre/*LoxP* or FLP/*FRT* system facilitates the production precise conditional mutations in all cells.

A CRISPR-Cas9 feeding system has been recently reported to generate conditional mutations in *C. elegans* (Liu et al., 2014). In this strategy, sgRNA is delivered by feeding bacteria that express sgRNA to the worms, which is similar to the RNAi feeding protocol. However, the efficiency of this strategy is limited compared to other approaches. In a direct comparison using the *dpy-5* locus, the somatic CRISPR-Cas9 method, in which the sgRNA is expressed under the control of P*U6* in P*dpy-5*::Cas9 animals, produced 91% Dpy animals, whereas the feeding system only produced the Dpy phenotype in 16% of the P*dpy-5*::Cas9 worms (Liu et al., 2014), which is even lower than the 79% Dpy defect produced by feeding *dpy-5* RNAi to the animals (Min et al., 2010). The *dpy-5* locus was the only gene examined using the CRISPR-Cas9 feeding system, and it remains unknown whether this system can efficiently generate conditional mutations in other genes or tissues.

Coronin Regulates Cell Migration in Live Animals

This study described the results of live cell imaging analysis in *C. elegans* conditional knockout larvae and revealed the functions of Coronin in neural development. Our previous study on Coronin examined the final positions of the Q cell progeny in adult worms (Cheng et al., 2013), and the present study directly depicted the dynamics of the actin cytoskeleton in WT and Coronin conditional knockout larvae. Our results indicated that Coronin acts with Cofilin to modulate F-actin organization in migrating neuroblasts, which is consistent with the findings from fibroblasts but was previously unknown in the nervous system. Importantly, these experiments demonstrated the feasibility of live cell imaging analysis of conditional knockout *C. elegans*

and will promote the application of these methods to examine organismal development at enhanced resolutions.

Mammalian Coronin 1, which is encoded at a genomic locus that is associated with neurobehavioral dysfunction, was reported to stimulate cAMP/PKA-dependent presynaptic plasticity by interacting with a G protein (Jayachandran et al., 2014). Our study suggested that the abnormality in neuronal positioning or neurite morphology might represent a previously unknown cellular origin of cognition and behavioral disorders. We showed that *C. elegans* Coronin regulates cell morphology and actin organization in migrating neuroblasts. In support of this finding, GFP-tagged Coronin is enriched in the leading edge or the growth cone of Q cells (Figures 7E and S4F; Movie S9), and 15% of the *cor-1* conditional knockout worms (N = 54) that were defective in Q cell migration developed misoriented neurites (Figures 7D and S4E). We found that the loss of function of COR-1 does not impede growth cone formation but affects its guidance (Figure 7D). Because growth cone formation requires the assembly of F-actin, a debranching factor of the actin network, such as Coronin, may be unnecessary for this process as long as the growth cone possesses a sufficient amount of G-actin for polymerization. However, growth cone guidance may rely on the debranching activity of Coronin to facilitate the constant reorganization of the existing actin network.

We found that 29% of the QR neuroblasts (N = 21) and 32% of the QL neuroblasts (N = 19) in the *cor-1-sg* conditional knockouts displayed an abnormally enlarged anterior portion, the penetrance of which was higher than the defects in the final position of the A/PQR neurons in these animals, suggesting that the cell morphology during migration is a more sensitive measure than the final position. In other words, other mechanisms may compensate for the defect in cell morphology during migration. Similarly, filopodia formation is more sensitive than the final axon guidance phenotypes; and in *unc-6* and *unc-40* mutants, the defects in filopodia formation are more severe than that in the final axon trajectory (Adler et al., 2006).

Mechanistically, Coronin 1 is thought to disassemble actin filaments via two pathways (Cai et al., 2007, 2008; Chan et al., 2011). First, by antagonizing the actin filament branch stabilizer Cortactin, Coronin 1 induces Arp2/3 complex dissociation and may serve to produce more flexible branches. Because the *C. elegans* genome does not encode a Cortactin homolog, the branch replacement function of worm COR-1, if it exists, may involve other factors. Second, by directing the phosphatase Slingshot to lamellipodia, where Slingshot activates Cofilin via dephosphorylation, Coronin 1 promotes the recycling of actin monomers to support continued actin polymerization at the leading edge. Our results suggest that a similar paradigm may apply to the neural development of living animals.

In summary, we developed an efficient and robust platform for conditional genomic modification in *C. elegans* somatic cell lineages. Via CRISPR-Cas9 targeted DNA cleavage, this methodology enables the functional analysis of embryonically lethal genes in postembryonic development and provides the capacity to separate the manifold roles of a single gene in multiple events. In principle, the presented platform is amenable to other model organisms and therapeutic applications in which efficient transgenesis is achievable. The simplicity of programming the CRISPR-Cas9 system to mutate specific genomic loci has enabled loss-of-function genetic screens on a genome-wide scale in mammalian cell lines (Shalem et al., 2014; Wang et al., 2014; Zhou et al., 2014). The somatic CRISPR-Cas9 technique displays the potential to support large-scale knockout screens in a conditional manner and to revolutionize functional genomics in multicellular eukaryotes.

EXPERIMENTAL PROCEDURES

The CRISPR-Cas9 and TALEN Constructs

The somatic CRISPR-Cas9 expression vectors were constructed by replacing the *eft-3* promoter in pDD162 (Addgene, #47549) with the *C. elegans* heat-shock promoter P*hsp-16.2* or a tissue-specific promoter using an In-Fusion HD cloning kit (Clontech). The sgRNA sequence was selected according to established criteria (Cong et al., 2013; Mali et al., 2013): the target sites conform to the sequence G(N)N19NGG (N = A, C, G, or T). The initial G optimizes the transcription driven by the U6 promoter, and the NGG (PAM) motif is required for Cas9 activity. We used the CRISPR design tool (http://crispr.mit.edu) to select the specific targets. To insert the target sequence into the somatic CRISPR-Cas9 vectors, the vectors were PCR-amplified using Phusion high-fidelity DNA polymerase (New England Biolabs) and the forward primer 5′-N17GTTTTAGAGCTAGAAATAGC-3′, in which N17 represents the 17 nt at the 3′ end of the N19 in the target sequence, and the reverse primer 5′-N17CAAGAACATCTCGCAATAGGA-3′, in which N17 is the reverse complement to the 17 nt sequence at the 5′ end of the N19 in the target sequence. To remove the vector template, the PCR products were digested with Dpn I (New England Biolabs) for 2 hr at 37°C and then transformed into TOP10 competent cells. The clones were verified to contain the target sequence via sequencing. For additional details, see Protocol. The construction of the TALEN plasmids was performed according to published protocols (Cheng et al., 2013; Huang et al., 2011). The TALEN binding sites, PCR templates, primers, and plasmid constructs are listed in the Supplemental Experimental Procedures.

C. elegans Strains, Genetics, and Heat-Shock Treatment

The *C. elegans* strains are listed in the Supplemental Experimental Procedures. All strains were raised at 20°C on nematode growth medium plates seeded with the *Escherichia coli* strain OP50. The PCR products and the DNA plasmids were injected into hermaphrodites using the selection marker P*odr-1::dsRed,* pRF4, *unc-76*-WT, P*egl-17::mCherry-Myri*, or P*egl-17::mCherry::TEV-S::his-24*. The injection concentration of the Cas9 and sgRNA plasmids was 50 ng/μl to generate the single conditional knockouts or 25 ng/μl to generate the double or triple conditional knockouts. *C. elegans* were heat-shocked at 33°C for 1 hr and then returned to 20°C. For additional details, see Protocol. The Dpy, Lon, and Unc phenotypes; the defects in the Q cell progeny; or the loss of GFP fluorescence were quantified at the adult stage (Cheng et al., 2013).

Molecular Analysis of the Mutations in the Conditional Knockouts

To detect molecular lesions induced by somatic TALENs or CRISPR-Cas9, transgenic worms at the L3 stage were lysed in 10× PCR buffer. The DNA fragment containing the TALENs or CRISPR-Cas9 targets was PCR amplified and purified using a MinElute gel extraction kit (QIAGEN, cat. no. 28606). Then, 800 ng of the DNA fragment was melted and reannealed to form heteroduplexed DNA. The resultant DNA was digested with 5 units of T7 endonuclease I (New England Biolabs) for 30 min at 37°C and analyzed via 2% agarose gel electrophoresis. Quantification based on the relative band intensities was calculated using ImageJ software (http://rsbweb.nih.gov/ij/). The indel percentage was determined according to the formula $100\times (1 - (1 - (b + c)/(a + b + c))^{1/2})$, where *a* represents the intensity of the intact band and *b* and *c* correspond to the integrated intensities of the digested small bands. To sequence the mutation, the PCR fragment was cloned into a pEASY-T1 Cloning Vector (Transgen, cat. no. CT101), and individual colonies were sequenced. For additional details, see Protocol. The primers used for molecular analysis are listed in Supplemental Experimental Procedures.

C. elegans Imaging

C. elegans were anesthetized using 0.1 mmol/L levamisole in M9 buffer, mounted on 2% agar pads and imaged at room temperature (20°C; Cheng et al., 2013). Our imaging system includes an Axio Observer Z1 microscope (Carl Zeiss MicroImaging) attached to a spinning disk confocal system (Yokogawa CSU-X1 Spinning Disk Unit). The images were acquired at exposure time of 300 ms using μManager (http://www.micro-manager.org). ImageJ software was used to process the images.

SUPPLEMENTAL INFORMATION

Supplemental Information includes Supplemental Experimental Procedures, five figures, nine movies, and one protocol and can be found with this article online at http://dx.doi.org/10.1016/j.devcel.2014.07.017.

AUTHOR CONTRIBUTIONS

G.O., Z.S., X.Z., Y.C., and W.L. conceived the experiments; Z.S., X.Z., Y.C., Z.Z., P.Y., and G.F. performed the experiments; and G.O. wrote the manuscript.

ACKNOWLEDGMENTS

We thank Drs. L. Cai, E. Lundquist, D. Huangfu, R. Korswagen, and M. Josephson for their comments. This study was supported by the National Basic Research Program of China to W.L. and G.O. (973 Program, 2013CB945600, 2012CB966800, and 2012CB945002); the National Natural Science Foundation of China to G.O., Y.C., and W.L. (31201009, 31222035, 31101002, 31301134, 31171295, and 31190063) and the Junior Thousand Talents Program of China to G.O.

Received: May 31, 2014
Revised: July 7, 2014
Accepted: July 21, 2014
Published: August 21, 2014

REFERENCES

Adler, C.E., Fetter, R.D., and Bargmann, C.I. (2006). UNC-6/Netrin induces neuronal asymmetry and defines the site of axon formation. Nat. Neurosci. *9*, 511–518.

Bloom, L., and Horvitz, H.R. (1997). The Caenorhabditis elegans gene unc-76 and its human homologs define a new gene family involved in axonal outgrowth and fasciculation. Proc. Natl. Acad. Sci. USA *94*, 3414–3419.

Branda, C.S., and Dymecki, S.M. (2004). Talking about a revolution: The impact of site-specific recombinases on genetic analyses in mice. Dev. Cell *6*, 7–28.

Cai, L., Marshall, T.W., Uetrecht, A.C., Schafer, D.A., and Bear, J.E. (2007). Coronin 1B coordinates Arp2/3 complex and cofilin activities at the leading edge. Cell *128*, 915–929.

Cai, L., Makhov, A.M., Schafer, D.A., and Bear, J.E. (2008). Coronin 1B antagonizes cortactin and remodels Arp2/3-containing actin branches in lamellipodia. Cell *134*, 828–842.

Capecchi, M.R. (2005). Gene targeting in mice: functional analysis of the mammalian genome for the twenty-first century. Nat. Rev. Genet. *6*, 507–512.

Chan, K.T., Creed, S.J., and Bear, J.E. (2011). Unraveling the enigma: progress towards understanding the coronin family of actin regulators. Trends Cell Biol. *21*, 481–488.

Cheng, Z., Yi, P., Wang, X., Chai, Y., Feng, G., Yang, Y., Liang, X., Zhu, Z., Li, W., and Ou, G. (2013). Conditional targeted genome editing using somatically expressed TALENs in C. elegans. Nat. Biotechnol. *31*, 934–937.

Chia, P.H., Chen, B., Li, P., Rosen, M.K., and Shen, K. (2014). Local F-actin network links synapse formation and axon branching. Cell *156*, 208–220.

Cong, L., Ran, F.A., Cox, D., Lin, S., Barretto, R., Habib, N., Hsu, P.D., Wu, X., Jiang, W., Marraffini, L.A., and Zhang, F. (2013). Multiplex genome engineering using CRISPR/Cas systems. Science *339*, 819–823.

Dickinson, D.J., Ward, J.D., Reiner, D.J., and Goldstein, B. (2013). Engineering the Caenorhabditis elegans genome using Cas9-triggered homologous recombination. Nat. Methods *10*, 1028–1034.

Ding, Q., Regan, S.N., Xia, Y., Oostrom, L.A., Cowan, C.A., and Musunuru, K. (2013). Enhanced efficiency of human pluripotent stem cell genome editing through replacing TALENs with CRISPRs. Cell Stem Cell *12*, 393–394.

Feng, G., Yi, P., Yang, Y., Chai, Y., Tian, D., Zhu, Z., Liu, J., Zhou, F., Cheng, Z., Wang, X., et al. (2013). Developmental stage-dependent transcriptional regulatory pathways control neuroblast lineage progression. Development *140*, 3838–3847.

Föger, N., Rangell, L., Danilenko, D.M., and Chan, A.C. (2006). Requirement for coronin 1 in T lymphocyte trafficking and cellular homeostasis. Science *313*, 839–842.

Friedland, A.E., Tzur, Y.B., Esvelt, K.M., Colaiácovo, M.P., Church, G.M., and Calarco, J.A. (2013). Heritable genome editing in C. elegans via a CRISPR-Cas9 system. Nat. Methods *10*, 741–743.

Frøkjær-Jensen, C. (2013). Exciting prospects for precise engineering of Caenorhabditis elegans genomes with CRISPR/Cas9. Genetics *195*, 635–642.

Gumienny, T.L., MacNeil, L.T., Wang, H., de Bono, M., Wrana, J.L., and Padgett, R.W. (2007). Glypican LON-2 is a conserved negative regulator of BMP-like signaling in Caenorhabditis elegans. Curr. Biol. *17*, 159–164.

Hall, D.H., and Hedgecock, E.M. (1991). Kinesin-related gene unc-104 is required for axonal transport of synaptic vesicles in C. elegans. Cell *65*, 837–847.

Huang, P., Xiao, A., Zhou, M., Zhu, Z., Lin, S., and Zhang, B. (2011). Heritable gene targeting in zebrafish using customized TALENs. Nat. Biotechnol. *29*, 699–700.

Jayachandran, R., Liu, X., Bosedasgupta, S., Müller, P., Zhang, C.L., Moshous, D., Studer, V., Schneider, J., Genoud, C., Fossoud, C., et al. (2014). Coronin 1 regulates cognition and behavior through modulation of cAMP/protein kinase A signaling. PLoS Biol. *12*, e1001820.

Joung, J.K., and Sander, J.D. (2013). TALENs: a widely applicable technology for targeted genome editing. Nat. Rev. Mol. Cell Biol. *14*, 49–55.

Kenyon, C. (1986). A gene involved in the development of the posterior body region of C. elegans. Cell *46*, 477–487.

Lieber, M.R. (2010). The mechanism of double-strand DNA break repair by the nonhomologous DNA end-joining pathway. Annu. Rev. Biochem. *79*, 181–211.

Liu, P., Long, L., Xiong, K., Yu, B., Chang, N., Xiong, J.W., Zhu, Z., and Liu, D. (2014). Heritable/conditional genome editing in C. elegans using a CRISPR-Cas9 feeding system. Cell Res. *24*, 886–889.

Mali, P., Yang, L., Esvelt, K.M., Aach, J., Guell, M., DiCarlo, J.E., Norville, J.E., and Church, G.M. (2013). RNA-guided human genome engineering via Cas9. Science *339*, 823–826.

Mello, C.C., Kramer, J.M., Stinchcomb, D., and Ambros, V. (1991). Efficient gene transfer in C.elegans: extrachromosomal maintenance and integration of transforming sequences. EMBO J. *10*, 3959–3970.

Miller, J.C., Tan, S., Qiao, G., Barlow, K.A., Wang, J., Xia, D.F., Meng, X., Paschon, D.E., Leung, E., Hinkley, S.J., et al. (2011). A TALE nuclease architecture for efficient genome editing. Nat. Biotechnol. *29*, 143–148.

Min, K., Kang, J., and Lee, J. (2010). A modified feeding RNAi method for simultaneous knock-down of more than one gene in Caenorhabditis elegans. Biotechniques *48*, 229–232.

Mueller, P., Liu, X., and Pieters, J. (2011). Migration and homeostasis of naive T cells depends on coronin 1-mediated prosurvival signals and not on coronin 1-dependent filamentous actin modulation. J. Immunol. *186*, 4039–4050.

Nonet, M.L., Staunton, J.E., Kilgard, M.P., Fergestad, T., Hartwieg, E., Horvitz, H.R., Jorgensen, E.M., and Meyer, B.J. (1997). Caenorhabditis elegans rab-3 mutant synapses exhibit impaired function and are partially depleted of vesicles. J. Neurosci. *17*, 8061–8073.

Pastrana, E. (2010). A toolset for the proficient geneticist. Nat. Methods *7*, 488–489.

Shalem, O., Sanjana, N.E., Hartenian, E., Shi, X., Scott, D.A., Mikkelsen, T.S., Heckl, D., Ebert, B.L., Root, D.E., Doench, J.G., and Zhang, F. (2014).

Genome-scale CRISPR-Cas9 knockout screening in human cells. Science *343*, 84–87.

Shiow, L.R., Roadcap, D.W., Paris, K., Watson, S.R., Grigorova, I.L., Lebet, T., An, J., Xu, Y., Jenne, C.N., Föger, N., et al. (2008). The actin regulator coronin 1A is mutant in a thymic egress-deficient mouse strain and in a patient with severe combined immunodeficiency. Nat. Immunol. *9*, 1307–1315.

Stringham, E.G., Dixon, D.K., Jones, D., and Candido, E.P. (1992). Temporal and spatial expression patterns of the small heat shock (hsp16) genes in transgenic Caenorhabditis elegans. Mol. Biol. Cell *3*, 221–233.

Sulston, J.E., and Horvitz, H.R. (1977). Post-embryonic cell lineages of the nematode, Caenorhabditis elegans. Dev. Biol. *56*, 110–156.

Suo, D., Park, J., Harrington, A.W., Zweifel, L.S., Mihalas, S., and Deppmann, C.D. (2014). Coronin-1 is a neurotrophin endosomal effector that is required for developmental competition for survival. Nat. Neurosci. *17*, 36–45.

Thacker, C., Sheps, J.A., and Rose, A.M. (2006). Caenorhabditis elegans dpy-5 is a cuticle procollagen processed by a proprotein convertase. Cell. Mol. Life Sci. *63*, 1193–1204.

Wang, X., Zhou, F., Lv, S., Yi, P., Zhu, Z., Yang, Y., Feng, G., Li, W., and Ou, G. (2013). Transmembrane protein MIG-13 links the Wnt signaling and Hox genes to the cell polarity in neuronal migration. Proc. Natl. Acad. Sci. USA *110*, 11175–11180.

Wang, T., Wei, J.J., Sabatini, D.M., and Lander, E.S. (2014). Genetic screens in human cells using the CRISPR-Cas9 system. Science *343*, 80–84.

Wiedenheft, B., Sternberg, S.H., and Doudna, J.A. (2012). RNA-guided genetic silencing systems in bacteria and archaea. Nature *482*, 331–338.

Wood, A.J., Lo, T.W., Zeitler, B., Pickle, C.S., Ralston, E.J., Lee, A.H., Amora, R., Miller, J.C., Leung, E., Meng, X., et al. (2011). Targeted genome editing across species using ZFNs and TALENs. Science *333*, 307.

Wu, X., Scott, D.A., Kriz, A.J., Chiu, A.C., Hsu, P.D., Dadon, D.B., Cheng, A.W., Trevino, A.E., Konermann, S., Chen, S., et al. (2014). Genome-wide binding of the CRISPR endonuclease Cas9 in mammalian cells. Nat. Biotechnol. *32*, 670–676.

Yang, H., Wang, H., Shivalila, C.S., Cheng, A.W., Shi, L., and Jaenisch, R. (2013). One-step generation of mice carrying reporter and conditional alleles by CRISPR/Cas-mediated genome engineering. Cell *154*, 1370–1379.

Zhou, Y., Zhu, S., Cai, C., Yuan, P., Li, C., Huang, Y., and Wei, W. (2014). High-throughput screening of a CRISPR/Cas9 library for functional genomics in human cells. Nature *509*, 487–491.